CFD Simulation and Flow Study of a Velocity Compounded Radial Re-Entry Turbine - Elektra

Fabian Janischowsky[1,*], *Dominik* Stümpfl[2,**], *Philipp* Streit[2,***], *Andreas P.* Weiß[2,****], and *Andreas* Lesser[1,†]

[1]OTH Regensburg, Turbomachinery Laboratory, Galgenbergstr. 30, 93053 Regensburg, Germany, +49 941 943 9965
[2]OTH Amberg-Weiden, Center of Excellence for Cogeneration Technologies, Kaiser-Wilhelm-Ring 23, 92224 Amberg, Germany, +49 9621 482 3531

Abstract. In order to meet the targets set out in the Paris climate agreement of 2015, the energy sector needs to be restructured. In Germany for example the goal is to move out of both nuclear and coal-fired power. In order to fulfil more demanding energy requests alternative sources of energy must be found and made available. One component is the usage of Waste Heat Recovery.
This paper deals with the evaluation simulation of an Elektra turbine, which concept is a velocity compounded radial re-entry single wheel turbine. Based on the first turbine design, multiple simulations were carried out in order to maximize the efficiency. With these simulations, optimization opportunities are described and identified. The paper concludes with a comparison of the results achieved by numerical simulation and on the experimental test bench. The main focus for this paper is to analyze the actual flow phenomena to identify possibilities for further improvements. All simulations were calculated with the commercial software FINE™/ TURBO 15.1.

*e-mail: fabian.janischowsky@oth-regensburg.de
**e-mail: d.stuempfl@oth-aw.de
***e-mail: ph.streit@oth-aw.de
****e-mail: a.weiss@oth-aw.de
†e-mail: andreas.lesser@oth-regensburg.de

1 Introduction and Motivation

With the purpose of slowing down the climate change, countries like Germany get out of nuclear and coal-fired power [1]. To generate electricity via a Rankine cycle, alternative heat sources like geothermal heat or waste heat need to be tapped. In comparison, these heat sources typically provide heat in a much smaller scale than conventional heat sources. In need of turbines dealing with these low temperatures, spoken in a power generating context, new concepts have to be developed to reach reasonable efficiency levels. In previous papers the usage of the Elektra turbine was evaluated [2, 3]. This turbine is velocity compounded and works according to the concept of a Curtis turbine, with the exception of only consisting of a single wheel with a radial re-entry. Therefore both velocity stages of the Curtis turbine are realised in the same wheel, which makes the Elektra much smaller and hence cheaper to manifacture, compared to the Curtis turbine.
The first Elektra invented by Otto Kolb, was built in 1905. This turbine implemented four wheel passes and is presented in Figure 1[4, p. 234].

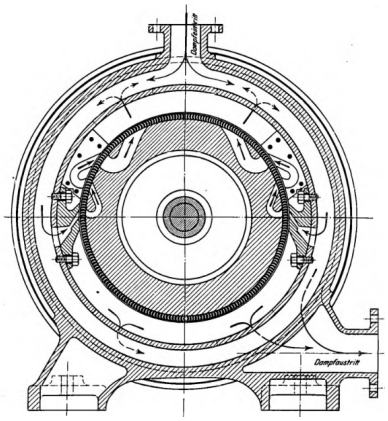

Figure 1: First built Elektra [4, p. 234]

2 Elektra Design

For the available test bench at the OTH Amberg-Weiden an air-driven Elektra with two wheel passes, according to one deflection channel, was built. The geometry of the first built version (V1) is presented in Figure 2. The turbine main design data is determined according to the capacity of the eddy current brake and the installed air compressors at the laboratory. These data is given in Table 1. The last four parameters of this table were calculated with a 1D-Turbine-Design-Tool (1DTDT) at the OTH Amberg-Weiden. [2]
In this paper the Elektra will be parted into four sections: Laval nozzle (Measuring points 0 and 1), deflection channel (2 and 3), outlet (4) and rotor. In the Laval nozzle the fluid is accelerated to supersonic flow. Its highest speed is expected to be close to measuring point 1. After the first wheel pass, the flow gets deflected and enters the wheel a second time, before exiting the turbine through the outlet.
In comparison to previous tests the geometry (V1 in [2]) was adjusted, as can be seen in Figure 3. The final geometry presented in this paper is counted as Version 7 (V7), because 5 other geometries have been tested since the initial geometry V1.
The most important changes are as follows:

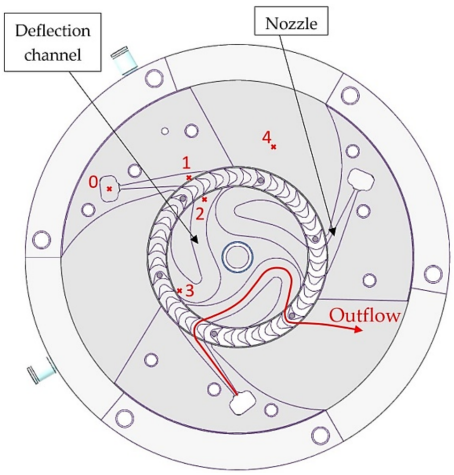

Figure 2: First Elektra design (V1) with the position of the pressure tappings (red cross) and the flow path (red line) [3]

Table 1: Turbine main design data [cf. 2]

Parameter	**Unit**	**Elektra air turbine**
Working fluid	-	pressurized air
Mass flow rate	g/s	65
Total inlet pressure	bar	10
Total inlet temperature	K	≈293
Static exit pressure	bar	≈1
Wheel diameter	mm	80
Rotational speed	rpm	29,000
Degree of admission	%	≈61
Pressure ratio	-	10
Nozzle exit Mach number 1DTDT	-	2.04
Rotor inlet relative Mach number 1DTDT	-	1.58
Expected efficiency η 1DTDT	%	64
Expected shaft power 1DTDT	kW	≈5

1. Laval nozzle: Several shock systems at the end of the Laval nozzle were detected, which indicates an overexpanded nozzle. Therefore the nozzle outlet width has been decreased. This leads to a decrease of the angle which the nozzle sweeps over the rotor from 19.2° to 15.5°, resulting in a lower degree of admission for the turbine.

2. Deflection channel: The deflecting direction of the channel has been changed. Therefore the fluid is first deflected and then flows through a straight channel. The fluid leaves the first rotor passage under highly unsteady and inhomogeneous conditions. The deflection in the channel also results in a inhomogeneous flow field since detaching of the flow is possible. Therefore it is easier to use the more turbulent flow to prevent detaching in the deflection channel by first deflecting it and after that homoge-

nize the fluid by using a longer and less curved channel. With this more homogeneous field it is easier to optimize the second rotor passage [5].

3. Outlet: In V1 a large mass flow rate leaving the nozzle directly to the outlet was detected, which does not contribute to the work of the turbine. To prevent this leakage the beginning of the outlet was shortened.

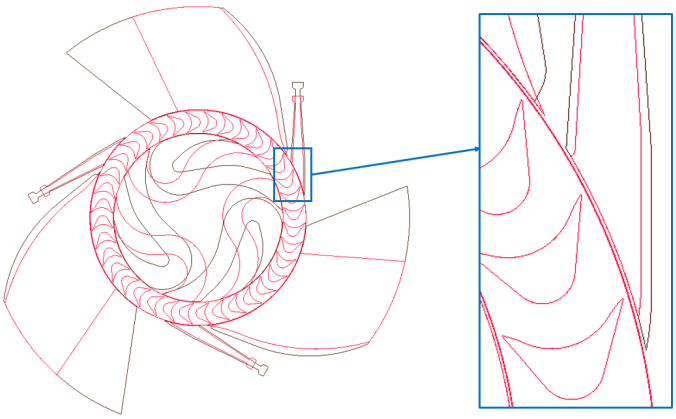

Figure 3: Comparison of initial (black) and final (red) geometry

3 Simulation Approach

The simulation model used for the different geometries is shown in Figure 4. Since the design in the Elektra is rotationally symmetrical, by 120°, it is suitable to only compute one third of the turbine with a periodicity of three. Additionally the inlet geometry was shortened. This is implied due to the assumption that the flow is homogeneous at the narrowest cross section of the Laval nozzle (Ma=1). Therefore only a small part of the geometrical inlet is needed to simulate the subsonic inflow.

Furthermore, compared to the geometry simplifications have been applied to the simulation model to achieve shorter simulation run times and a more stable behaviour. Therefore the tip clearances between rotor and stator, which will lead to a mass flow rate above and below the rotor, were neglected. The chosen Rotor-Stator-Interfaces (RS-Interface), see Table 2, require the same periodicity between rotor and stator. Therefore a 120° stator block (blue in Figure 4) on each side of the Rotor has to be implemented. The thickness of these RS-Interface Blocks can be chosen according to the radial gap between rotor and stator.

The chosen parameters for the steady and unsteady simulations are given in Table 2. The Spalart-Allmaras turbulence model is used in order to further reduce the computing time. The extended wall functions need to be used, since the first cell height is at 1×10^{-5} m, which results in a y_+ of about 20 to 30 at the end of the Laval nozzle. The time step is chosen according to 20 Positions for each blade passage, to evaluate the differences in the flow through the turbine depending on the rotor position. In a rotor with 12 meshed blades (respectively 36 blades in the geometry) this results in 20 positions $\cdot$ 12 blades $=$ 240 time steps per rotation over 120°. The unsteady simulation is carried out with as many periods as

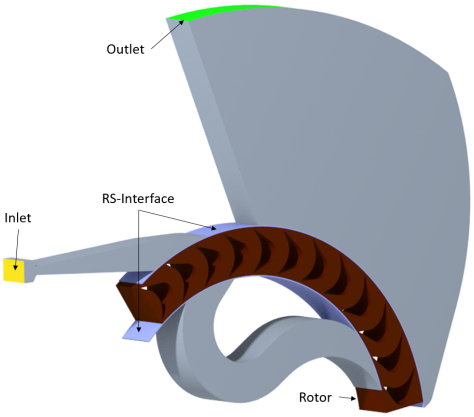

Figure 4: Simulation model

needed until the simulation could be accounted as converged. This convergence is achieved as soon as the difference between the actual and the previous period is no more visualizable. It is typically reached after 7 to 10 periods.

Table 2: Simulation Parameters

Category	Parameter	Value
Flow model	Fluid	Air (perfect gas)
	Turbulence model	Spalart-Allmaras with extended wall function
	RS-Interface	Full non matching frozen rotor (steady), domain scaling (unsteady)
Boundary conditions	Inlet	Subsonic, total pressure (p_t = 1,000 kPa), Total temperature (T_t = 293.15 K)
	Outlet	Subsonic Averaged static pressure (p_0 = 100 kPa)
	Walls	Solid, adiabatic
	Rotational speed	29,000 rpm
Numerical control	Time stepping	0.5° per time step
	Number of periods	7

Since the turbine is only partially admitted, highly unsteady behaviour and phenomena are to be expected. Therefore the results of a steady simulation are only used to initialize its unsteady simulation.

4 Flow Study

In the following pictures instantaneous results are shown. The cutting plane is placed at 50 % of the nozzle height. The absolute M ach number for the final geometry version is plotted in Figure 5. The main part of the fluid (red arrows) flows as expected through the first rotor passage, to the deflection channel, through the second rotor passage and into the outlet. The

exact mass percentage, which follows this route depends on the leakage mass flow rates, which are highly influenced by the geometry of the deflection channel. In every simulated geometry this leakage accounts to up to 25 %. Due to the occurrence of such high leakages its origins shall be identified to analyze where further improvement is possible.
In the final geometry (V7) four leakage mass flow rates (pink arrows) were detected. The listing relates to the numbers in Figure 5.

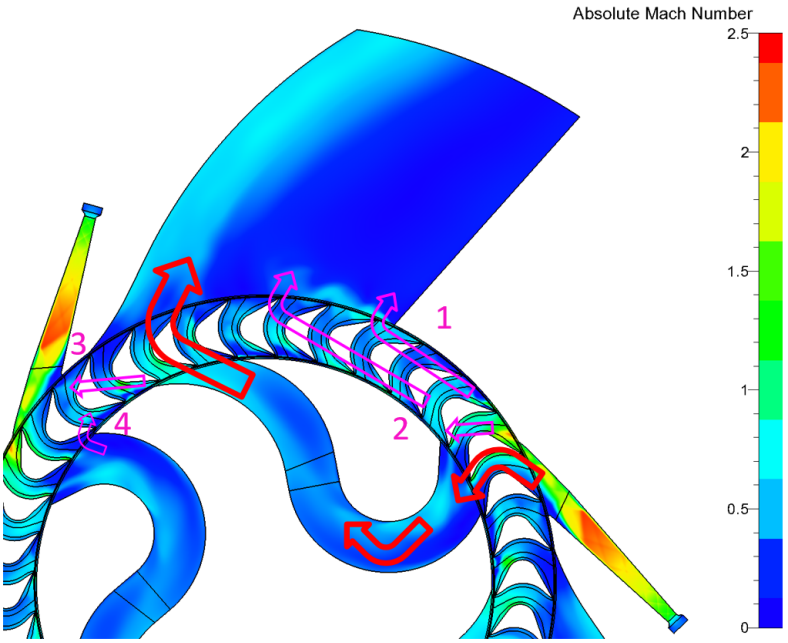

Figure 5: Absolute Mach number distribution of the final geometry V7

1. The first leakage has its origin in the gap between rotor and stator. Here the flow leaves the nozzle and is not able to enter the rotor, but is flowing over the rotor and directly to the outlet. This mass flow rate therefore has no significant contact with any blade and hence does no work.

2. The second leakage mass flow rate follows the main stream through the first rotor passage, but is not able to reach the inlet of the deflection channel. During the time, while the fluid is flowing through the first blade passage, the rotor rotates a couple degrees and transports the fluid in circumferential direction. As the fluids velocity is too slow or the rotational speed is too high, a fraction of the turbines mass flow rate hits the inner wall of the rotor. The fluid of this mass flow rate stays in the rotor and is pressed outwards during the rotation, because of the existence of centrifugal forces. The fluid leaves the rotor approximately in the middle of the outlet right between the first leakage mass flow rate and the main flow.

3. The third leakage mass flow rate is similar to the second one but for the second rotor passage. The fluid enters the second rotor passage after flowing through the deflection channel, but is not able to reach the outlet in time. It then has to remain in the rotor and is pressed against the Laval nozzle, where it is accelerated into the rotor and flows back to the inside of the deflection channel.

4. The fourth leakage mass flow rate occurs in the deflection channel. It leaves the deflection channel through its inlet and flows against the rotational direction through the rotor to the outlet of the deflection channel. There it meets the third leakage mass flow rate and again hits the Laval nozzle. Hence the third and fourth mass flow rate never leave the turbine but keep fluctuating between deflection channel, rotor and nozzle and are therefore accounted as recirculation areas.

Both recirculations (3 and 4) are critical for the nozzle flow, since they now tend to stream inside the nozzle. This results in an early detaching point on the streamwise left side of the nozzle (Point 5 in Figure 6). Most of the mass flow rate of the Laval nozzle is shifted to the right side, since there is no resistance from instreaming mass flow rates. As a result the flow condition of the nozzle is shifted, because it is no longer homogeneous streamed through, but tipped to the right. This tipping is shown in Figure 6.
At point 6 another effect is visualized. Here the Mach number increases locally to around 3 to 4. In this area exists the fastest flow of the Elektra turbine. It depends on the rotor position and only occurs when a blade is reaching the end of the Laval nozzle and cuts off the mass flow rate coming from the nozzle. Hence at this time a small second Laval nozzle is created, which accelerates the flow and results in the existence of another shock system at around 30 % chord length.

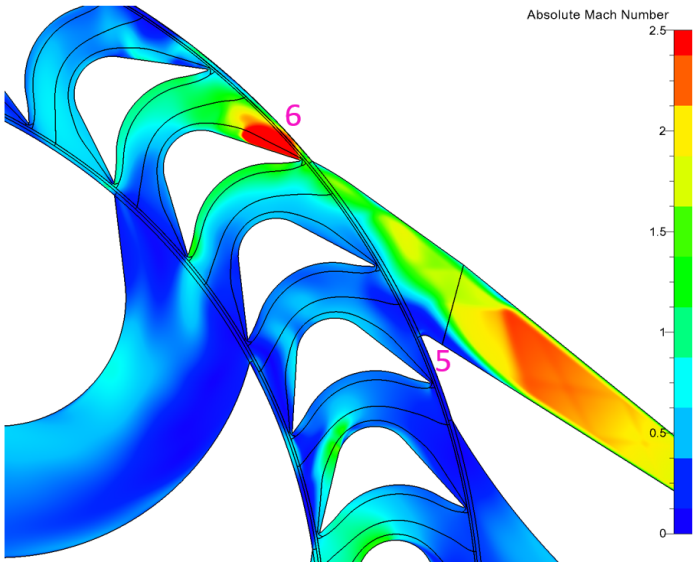

Figure 6: Absolute Mach number distribution of the final geometry V7 at the first rotor passage

In Figure 7 the static pressure is shown. The static pressure for the nozzle outlet (Point 7) is higher as intended at the design conditions (100,000 Pa). Therefore the nozzle cannot expand to the outlet pressure but has to find a condition, where at its outlet it meets a static pressure of approximately 200,000 Pa. This occurs due to pressure losses in both rotor passages and a high pressure state in the deflection channel. The losses lead to the difference in the static pressure between nozzle outlet and turbine outlet, where the boundary condition predefines a static pressure of 100,000 Pa.

Both, the mass flow rate in the nozzle and the high pressure at its outlet, result in bad conditions for the nozzle itself, which leads to the occurrence of a large shock system at around two-third of the length of the nozzle. According to the 1DTDT the nozzle outlet Mach number should be at 2.0 (see Table 1), the simulated Mach number at the nozzle exit is, with around 1.4, significantly lower.
The high static pressure in the deflection leads to another effect presented at point 8 in Figure 7. In this area fluid from the deflection channel is sucked into the rotor, streams against the rotational direction and collides with the second leakage mass flow rate. The suction occurs since the static pressure in the deflection channel is significantly higher than the static pressure in the rotor in that area. The static pressure of the rotor is decreasing while rotating through the outlet area, because fluid is transported from the rotors inner radius to the outlet due to circumferential forces. The collision of both mass flow rates leads to a dissipation indicated by an increase in the entropy as presented in Figure 8. This fluid with high entropy is then mixed in the rotor with more fluid streaming from the deflection channel.

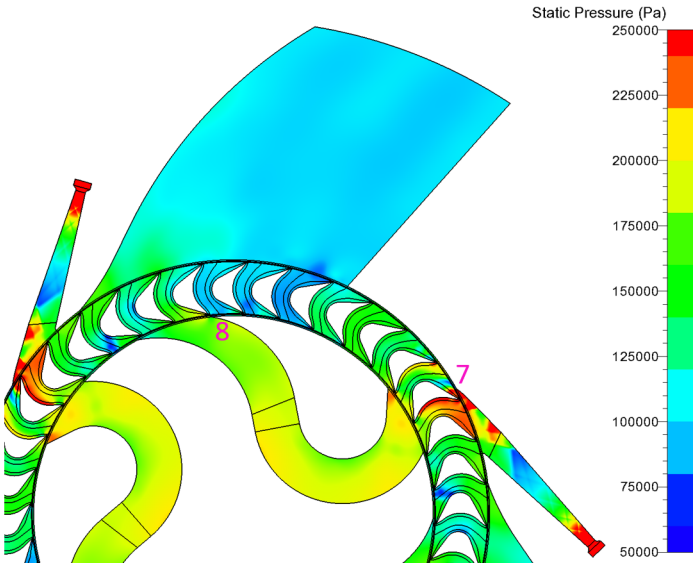

Figure 7: Static pressure distribution of the final geometry V7

Furthermore two more areas with entropy production in the turbine exist, marked with numbers 9 and 10. At Point 9 the leakage mass flow rates 3 and 4 collide and increase the entropy at that position. The fluid with high entropy enters the Laval nozzle, is accelerated through the rotor passage and mixes again with the main flow in the deflection channel.
At point 10 the second Laval nozzle leads to a shock system and hence increases the entropy in the area where the shock occurs. The fluid with high entropy flows in rotational direction with the rotor and leaves the system through the outlet. The entropy in the outlet appears to be lower than at the shock position due to mixing processes with the mass flow rate from the deflection channel.

The appearance of this amount of unsteady phenomena assures the need to only evaluate unsteady simulations.

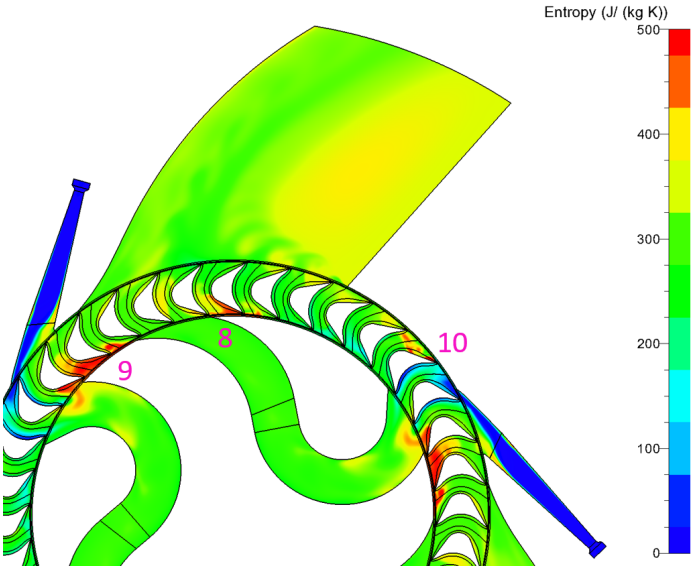

Figure 8: Entropy distribution of the final geometry V7

5 Comparison

Both geometries, V1 and V7, were manufactured and tested on the compressed air test bench of the OTH Amberg-Weiden. The specifications of the test bench are described in [3]. The efficiency is calculated according to Equation 1:

$$\eta = \frac{2 \cdot \pi \cdot n \cdot M}{\dot{m} \cdot c_p \cdot T_{in} \cdot \left[\left(\frac{p_{s,out}}{p_{t,in}}\right)^{\frac{\kappa-1}{\kappa}} - 1\right]} \tag{1}$$

Where n is the rotational speed, M the torque, $\dot{m}$ the mass flow rate, c_p the specific heat capacity, T_{in} the inlet temperature, $p_{s,out}$ the static pressure at the turbine outlet, $p_{t,in}$ the total pressure at the turbine inlet and κ the heat capacity ratio.
In Figure 9 the measured efficiency depending on the pressure ratio, between inlet and outlet, and the rotational speed for initial and final geometry is given. The green curve describes the calculated efficiency in the simulation for different simulated rotational speeds. First to be noted is that the pressure ratio is not identical but in the range between $PR = 10 - 10.4$. Hence the results for the same PR might differ, but are still considered as comparable. This is justified by the influence on the change of efficiency being significantly higher with the geometry changes than with the pressure ratio differences. Therefore most fraction of the difference between the curves is related to the geometry while the pressure ratio difference is only responsible for a minor portion of efficiency change. Nevertheless the efficiency for the final geometry compared to the initial geometry increased, but its amount is depending on the rotational speed.
The maximum efficiency for the initial geometry was measured at 35,000/min at 33 %.The efficiency for the final geometry reaches a plateau between 22,500/min and 32,500/min at 36.0−36.5 %. As in both cases the design point of the turbine is at 29,000/min the highest efficiency should have been at that rotational speed.
The comparison of both curves leads to the conclusion that the final geometry results in a

6 %p higher efficiency than the initial geometry until its plateau at 22,500/min is reached. After that the efficiencies merge together resulting in a higher efficiency for the final geometry at 37,500/min of 2 %p. The shift to a maximum efficiency at lower rotational speed was observed to highly depend on the geometry of the deflection channel.

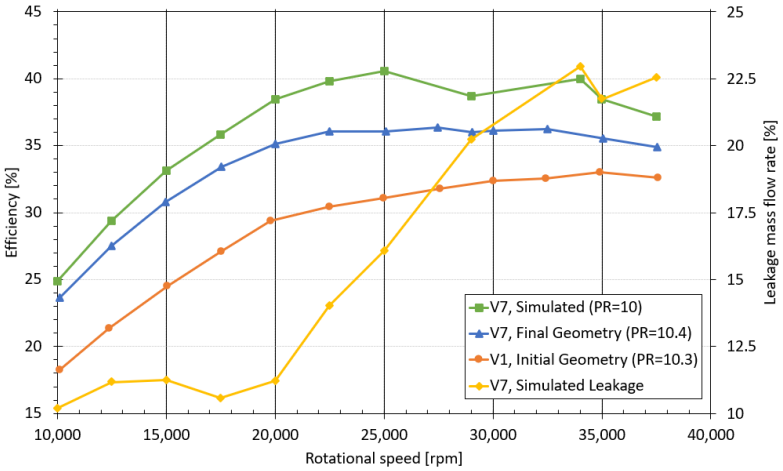

Figure 9: Comparison of efficiency initial geometry vs. final geometry

In the simulation the leakage mass flow rate between V1 and V7 increased from 15 % to 21 % at 29,000/min. The increase in the leakage mass flow rate corresponds to the shift of the point of the highest efficiency to lower rotational speeds. The assumption is, that for lower rotational speeds a higher percentage of fluid is able to enter the deflection channel. Hence the leakage mass flow rates 2 and 3 decrease, since they exist only due to the rotation of the rotor. This assumption is supported by the fact, that the overall massflow leakage increases from 20,000/min at 11 % to around 22 % for the highest rotational speeds, as can be seen in Figure 9. If the rotational speed is increased both losses (2 and 3) increase proportionally and therefore have a more negative impact on the overall efficiency. The comparison of the initial geometry and the final geometry in Figure 3 shows, that the inlet of the deflection channel is larger for the initial geometry and hence reduces leakage mass flow rate 2. The same concept applies for the channels exit with leakage mass flow rate 3. Here the offset between channel outlet and turbine outlet is reduced for the final geometry. For the same velocity the fluid has less time to leave the rotor and enter the turbine outlet. Since the leakage mass flow rate 3 also shifts the Laval nozzles state to earlier shocks and lower Mach numbers, its impact on the turbines efficiency might be relatively huge.
For the comparison of the measured efficiency with the simulated efficiency, the same efficiency definition as in Equation 1 is used. It is clear that the simulation overestimates the measurement by up to 4 %p. This effect is expected since in the simulation some negative effects such as manufacturing inaccuracies, bearing friction or disc friction are ignored. Although the measured efficiency has to be lower than the simulated one, it is still possible that there are additional effects, that influence the turbine on the test bench.

6 Conclusion

In the flow study for the current version of the Elektra turbine 10 different flow phenomena have been identified. Since they all affect the turbine efficiency in a negative way they have to be targeted for further improvements. Comparing the two geometries, the V7 performs significantly better than the V1. For higher rotational speeds its advantage shrinks but still remains by a couple percentage points. The worse performance at higher rotational speeds can be explained by the increased leakage mass flow rates.
Especially the mass flow leakage rates 3 and 4 have a significant impact on the nozzles flow condition and shift the turbine to new, unwanted states. To further verify that assumption it is necessary to find a measurement method that could record the percentage of the leakage mass flow rates during the tests. The simulation model seems to be sufficient to predict the performance of the Elektra turbine. This model could be improved by the usage of hub and shroud gaps in order to simulate the overflowing fluid which will lead to a higher mass flow leakage than the one which is currently simulated. If the assumption for the mass flow leakage is verified, these leakages have to be tackled with in future geometries. Since these losses currently equal a fourth of the turbine's mass flow rate there seem to be many possibilities for improvement.
The geometry of the deflection channel shows high impacts on those leakages and therefore should be improved in a first step. This could be done by for example widening the inlet of the deflection channel in order to reduce mass flow leakage 2. Another option would be to increase the tolerances for the offsets in both rotor passages. By varying the deflection channels inlet and outlet position the mass flow leakages 2 and 3 could be reduced even further. With these improvements the static pressure inside the deflection channel should be decreased leading to reduced outflows in the rotor which should then reduce the mass flow leakage 4 and the entropy increase at phenomenon 8. Concluded the position and angles of the deflection channel leads to most of the described phenomena, therefore a better channel should reduce the mass flow leakages back to around 11 % and increase its efficiency for higher rotational speeds. The mass flow leakage 1 according to the second Laval nozzle (phenomenon 6 and 7) seem to be of a lesser order and should therefore be tackled only after these improvements.

References

[1] Sterchele P., et al., *Paths to a climate-neutral energy system* (Fraunhofer Institute for Solar Energy Systems ISE, Freiburg, 2020)

[2] Weiß A. et al., *Uncommon turbine architectures for distributed power generation - development of a small velocity compounded radial re-entry turbine* (Archives of thermodynamics, 2020)

[3] Weiß A. et al., *Numerical and Experimental Investigation of a Velocity Compounded Radial Re-Entry Turbine for Small-Scale Waste-Heat-Recovery* (MDPI Energies, 14., 2021) (DOI: 10.3390/en15010245)

[4] Kolb O., *Dampf-Turbine* (1900, Patent-Nr. AT000000003865B, Kaiserlich königliches Patentamt)

[5] Sautereau M., *Numerische Optimierung des Umlenkkanals einer Elektra-Turbine* (Master thesis at OTH Regensburg, 2021)